Original Research Article: full paper

(2023), «EUREKA: Physics and Engineering»
Number 1

A NUMERICAL RESEARCH ON THE INTERACTION BETWEEN UNDERWATER EXPLOSION BUBBLE AND DEFORMABLE STRUCTURE USING CEL TECHNIQUE

Anh-Tu Nguyen
Faculty of Mechanical Engineering
Hanoi University of Industry
298 Cau Dien str., Hanoi, Vietnam, 100000
tuna@haui.edu.vn

Abstract

The dynamic process of an underwater explosion (UNDEX) bubble in the vicinity of deformable structures is a complex phenomenon that has been studied by many researchers. The dynamic process of a UNDEX bubble is a complex transient problem that results in a highly distorted bubble and large deformation of the structure. The previous work has introduced various solutions for studying the interaction between the UNDEX bubble and deformable structure. The interaction between the bubble and nearby structures has been widely solved by the combination of the boundary element method (BEM) and the finite element method (FEM). However, this couple requires tight time-step controlling, long-time analysis, and large computer resources. Furthermore, this combination is not widely used as the FEM code in commercially available software for solving UNDEX bubble problems. This paper presents a coupled Eulerian-Lagrangian (CEL) approach in commercial software to deal with the fluid-structure interaction (FSI). The numerical model of a UNDEX bubble is first developed and verified by comparing results with experimental, BEM, and empirical data. Then both bubble behavior and structural deformation are examined in various case studies. The numerical results show that the stiffness of the structure has strongly influenced the bubble behavior and the water jet development. The pressure pulse becomes significantly large as the bubble collapse. Besides, this numerical approach also can reproduce crucial phenomena of a UNDEX bubble, such as the whipping effect and water jet attacks. Although the numerical model is developed using simplified boundary conditions, the proposed approach shows the feasibility of simulating the important features of a UNDEX bubble process as well as the response of nearby structures.

Keywords: UNDEX bubble, Fluid-structure interaction, CEL technique, finite element method, Water jet.

DOI: 10.21303/2461-4262.2023.002637

1. Introduction

An underwater explosion is normally classified into two major and distinct phenomena. The shockwave propagates in a very short time and a following detonation gas bubble oscillates in a longer duration at high temperature and high pressure [1]. The dynamics of the bubble involve the pulsation process and collapse phase, along with the development of a high-speed water jet. Recent advances in computers have helped model and simulate the UNDEX bubble phenomenon faster and more accurately while saving computational resources. Furthermore, the computational modeling can predict various features of the bubble and provide valuable data that is difficult to investigate by doing explosions. BEM is a numerical method that solves the governing equations in the integral form. In the BEM model, only surface elements are discretized and applied boundary conditions, therefore this method consumes less time and fewer computational resources for analysis. Besides, this technique allows changing mesh and performing re-mesh easily with high accuracy. These features make BEM more efficient in dealing with bubble dynamics problems. A 3D model of two bubbles parallel to the free water surface was developed for studying the dynamics. This method allows computing solid angles on the free surface [2]. In another study, a nonlinear distribution of nodes was applied on the free surface to determine the spike motion. This enhancement could accurately capture the motion of one bubble near a free surface [3]. During the collapse period, the bubble develops into a toroidal form and induces flow circulation. To account for this velocity potential of the bubble, a method using a vortex ring has been introduced and applied in numerous studies [4−6]. Then, the vortex ring theory was extended by combining it with a smooth scheme for the 3D model. This approach can compute the flow in the toroidal phase and simulate the dynamics

of 3D bubble models [7]. After that, the vortex ring technique has been developed into multiple models, which allows simulating the interaction between two or more toroidal bubbles. The results showed a high pressure occurring at the splitting region [8]. To overcome the high distortion of the mesh during the simulation, an elastic mesh technique (EMT) has been incorporated in the boundary integral method (BIM), this combination allows maintaining the stable and smooth mesh without doing mesh refinement during the bubble evolution [9]. In an attempt to reduce the computing time, a 2D numerical model of the bubble was developed using the Arbitrary Lagrange Euler theory. The entire pulsating process of the UNDEX bubble was successfully simulated. The proposed method was corroborated by the comparison with empirical and theoretical calculations [10]. Another approach for dealing with the UNDEX bubble problem that should be cited here is the combination of the LS-DYNA software and BEM. In which, the LS-DYNA software was applied to simulate the initial explosion while the BEM was used for solving the bubble dynamics. The proposed method was validated by the experiment [11].

The dynamic process of a UNDEX bubble is a complex transient problem that results in a highly distorted bubble and large deformation of the structure. The combination of BEM and FEM codes has been widely used by researchers for solving the FSI, in which the FEM calculates the structural response, and the BEM computes the motion of the flow [12−14]. An approach by matching the pressure and velocity parameters for coupling the fluid and structure was introduced [12]. The analysis showed that the bubble behavior is affected strongly by the nearby rigid structure motion. By combining the BEM and FEM, the case of a UNDEX bubble interacting with a flat plate, a cylinder, and a ship was analyzed. The results investigated that the maximum stress occurs on the structure at the bubble collapse and the whipping effect occurs at the low order eigenfrequency of the ship [13]. The BIM was successfully integrated with FEM for developing a 3D model, this method allowed studying the bubble pulsation in different boundary conditions: fixed, rigidly moving, and flexible structures [14]. A fully coupled 3D model of a bubble interacting with a structure was established by coupling BEM and the explicit finite element method (EFEM). The analysis pointed out that the approach is more stable than the loosely coupled model [15]. In another study, the BIM was used to develop models of a gas bubble nearby a rigid wall and a complicated surface. The effects of bubble jet load were explored and compared well with experimental results [16]. Recent works based on the combination of BEM and FEM have the permit to study the deformation of a simplified ship due to the UNDEX bubble dynamics. The effects of standoff distance on the structure deformation have been analyzed and well compared to experimental results [17, 18]. The elastic and plastic deformation of a plate subjected to the UNDEX bubble has also been examined in the consideration of the fluid flow affecting both sides of the structure [19].

A useful approach for solving FSI has been addressed, in which a «negative mirror» method was applied for simulating the bubble behavior near both the free surface and floating structure. The comparison showed a good agreement with the results obtained by exiting axial symmetrical code [20]. A complex combination of the Euler theory, 5 steps Adams-Beshforse method, and 4 step Adams-Moltone approach was developed for solving the response of ship structure caused by oscillation bubble. By analyzing the stress occurring on the ship, the influence of explosion depth and explosive mass was investigated [21]. Recently, the combination of the Runge-Kutta discontinuous Galerkin method (RKDG) and BEM was introduced to establish a numerical model of a UNDEX bubble near a rigid wall. All oscillation processes, collapse phases, and bubble-jet processes were successfully simulated. The development of high-speed water jets nearby vertical and horizontal walls was considered at different stand-off distances [22]. To obtain sufficient knowledge about the UNDEX phenomenon, numerous scientists examined the behavior of the bubble in the different boundary conditions. The RKDG method was coupled with BEM and FEM for studying the effects of the deformation of sandwich structures on bubble behavior [23]. In another research, the interaction between the UNDEX bubble and lightweight corrugated sandwich plates (LCSP) was investigated based on the MSC. Dytran Software. The bubble shape, impact pressure, and fluid field velocities were examined at different stand-off distances. The results indicated that the jet load in the bubble collapse plays an integral role in the near-field underwater explosion [24]. In an attempt to manage the development of the jet, the effects of the plate velocity, standoff distance, and the

scale of a moveable sandwich plate on the bubble behavior were examined. The results showed that the structure with large deformation and high-speed deformation like a sandwich plate can alter the jet direction [25]. Recently, a numerical model using a double-vortex model was proposed for solving the doubly connected bubble. This model was also accompanied by the mode-decomposition method for calculating the FSI. The influence of both buoyancy and distance parameters on bubble oscillation, jet attack, and slamming load produced by the waves were investigated [26]. A novel approach that should be cited here is a hybrid algorithm. This method was developed by combining the BEM and smoothed particle hydrodynamics (SPH) to simulate the detonation process of a column charge near a rigid wall. The close comparison between numerical and experimental results has proven that this approach can study the UNDEX bubble problem [27].

The previous work has introduced various solutions for studying the interaction between the UNDEX bubble and deformable structure. The combination of the BEM and FEM codes has emerged as a popular method among researchers and provided valuable information. However, the drawback of this approach is that it requires controlling time steps tightly during the analysis and is complicated to operate. Besides, this combination is not widely used as the FEM code in commercially available software for solving UNDEX bubble problems. The ALE method shows advantages in solving FSI since it straightforwardly couples fluid dynamics to structural dynamics, therefore avoids using a separate coordinate coupling module. However, the ALE method uses matching element nodes for coupling two regions, this prevents Lagrangian to collapse if the material is entrained between two regions, and therefore restricts the method to apply for bubble jet problems [28]. The CEL approach utilizes the advantages of both Eulerian and Lagrangian theories. The Lagrangian elements continuously interact with the Eulerian domain, this allows true coupling of the fluid and structure. Besides, the CEL approach allows including the Lagrangian material within Eulerian calculation, this helps overcome difficulties of calculating partially filled cells. Furthermore, the Lagrangian mesh can be rezoned into the Eulerian mesh, this allows converting the distortion materials into an Eulerian computation. This method is suitable for high-velocity impact problems. The present paper applies the CEL technique in a FEM commercial software for solving the FSI, in which the detonation gas, air, and water are simulated using the Eulerian technique and the deformable structures are simulated using the Lagrangian theory. The effect of the stiffness of the wall on the bubble behavior and the development of the water jet is examined. Besides, major features of the bubble oscillation are reproduced in various case studies, and the structural deformation of the nearby structure is also determined. Results so far have revealed that the proposed method is applicable for further study of the UNDEX bubble phenomena.

2. Materials and methods

2. 1. Coupled Eulerian-Lagrangian technique

To study the dynamic FSI in impact problems, using a single approach can only investigate certain facets of the process while the UNDEX bubble involves numerous phenomena. The Lagrangian technique is widely used in simulating solid structures because the nodes and the flow of materials move together during the deformation. This method helps easily apply boundary conditions and tracts the nodal displacement. However, the major limitation of the Lagrangian method is that the model elements may become overly distorted when the high strain gradients occur during the analysis. This could cause the short-time step and reduce the accuracy of results.

Inversely, the Eulerian method is well-suited for simulating large deformation or fluid dynamics. In this approach, the nodes remain fixed during the analysis and the materials move inside the mesh, this allows simulating multi-material in the same element. Nevertheless, the drawback of this approach is that it is difficult to track the motion of materials and apply the constraints on the boundary surfaces. Besides, the Eulerian technique consumes larger computing time and computational memory. **Fig. 1** illustrates the deformation of Lagrangian and Eulerian materials during the analysis.

ABAQUS/Explicit provides a CEL technique for solving the FSI problems, in which the Eulerian and Lagrangian elements are assembled in a model. The Eulerian meshes are fixed and covered by the Lagrangian meshes. The flow of Lagrangian materials is constrained into the Eulerian domain and the pressures are transmitted from the Eulerian grids to Lagrangian grids at the

interface of two domains. Therefore, the Lagrangian grids play as a geometric boundary of the material flows to the Eulerian grids. When the Lagrangian meshes deform or move, they may overlap the Eulerian meshes or not. ABAQUS applies the penalty method for the Eulerian-Lagrangian contact constraints [29].

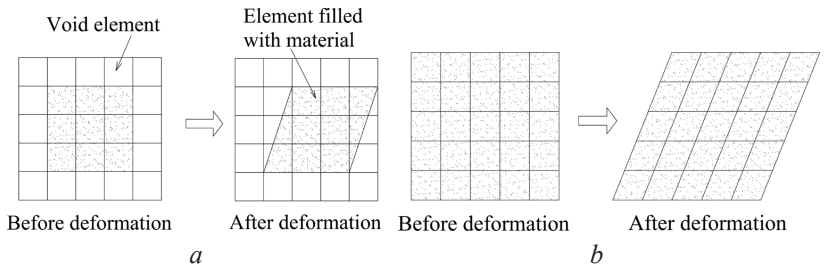

Fig. 1. The deformation of Lagrangian and Eulerian grids during the analysis: *a* – Eulerian analysis; *b* – Lagrangian analysis

The combination of Eulerian and Lagrangian cells is described in **Fig. 2**, in which the Lagrangian elements and the Eulerian domain continuously interact with each other in a model [30]. The communication between two regions is accomplished through the interface elements that are coincided with the outside Lagrangian surface.

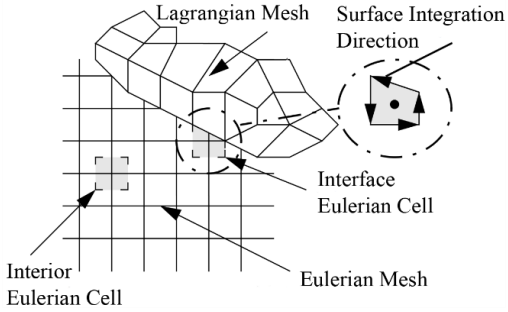

Fig. 2. Combination of Eulerian and Lagrangian elements [32]

Fig. 3 illustrates the schematic diagram of the penalty method for the case of a Lagrangian node lying within an Eulerian cell at the time step t_n (**Fig. 3**). The displacement of the Lagrangian mesh is first determined using the current pressure in the Eulerian domain. Then the motion of the Eulerian material is calculated based on the updated position of the Lagrangian element. Finally, Lagrangian and Eulerian nodes are applied the penalty force for further calculation.

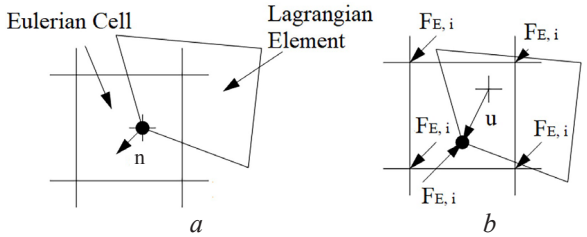

Fig. 3. Coupled Eulerian-Lagrangian [25]: *a* – at the time step t_n; *b* – at the time step t_{n+1}

The penalty force is defined as [26]:

$$F_p = k_p u_p, \tag{1}$$

where k_p is the penalty stiffness and u_p is the penalty displacement.

If the relative motion between two domains is compressive, the penalty displacement is calculated using interface friction as following:

$$u_p = \begin{cases} u_n & \text{if} \quad f_f = 0, \\ u_n + f_f \dfrac{|u_t|}{|u_n|} u_t & \text{if} \quad |u_n| < f_f |u_t|, \\ u & \text{if} \quad |u_n| \geq f_f |u_t|, \end{cases} \tag{2}$$

where f_f is the coefficient of friction, u_n and u_t are the normal and tangential components of the actual displacement vector, u. These components are determined as:

$$u_n = (u \bullet \vec{e})\, \vec{e},$$

$$u_t = u - u_n,$$

where $\vec{e}$ is the outward-directed normal vector to a Lagrangian surface at a Lagrangian node.

The penalty stiffness is defined as:

$$k_p = \beta \frac{m}{\Delta t^2}, \tag{3}$$

where β is a multiplier, Δt is time step interval, and m is the minimal value of the Lagrangian mass, m_L, and Eulerian mass, m_E.

Since the penalty force is determined, the applied force at the i-th Elerian node can be calculated using:

$$F_{E,i} = E_i \alpha_i F_p, \tag{4}$$

where E_i is the Eulerian basis function estimated at the position of the Lagrangian node at the end of the time step, α_i is the weight function depending on Eulerian mass at each node, $m_{E,i}$:

$$\alpha_i = \min\left\{1, \frac{m_{E,i}}{(E_i + 0.001)m}\right\}. \tag{5}$$

The force exerted on each Lagrangian node is based on the Eulerian forces as:

$$F_L = -\sum F_{F,i}. \tag{6}$$

2. 2. Numerical bubble model

In this section, the numerical model of a bubble in the free field has been first developed and validated by estimating the numerical data with the corresponding validated results from experiments, BEM, and empirical calculation. The simplified numerical model is replicated an experimental bubble in a pond, in which the charge weight was positioned at the pond middle [31]. The UNDEX phenomenon includes two distinct periods, the shock wave transmission, and the bubble pulsation, since the duration of bubble migration is much longer than that of the shockwave transmission, the influence of the shockwave is eliminable when studying bubble dynamics. The initial bubble is supposed to be spherical, and the detonation gas is considered as an ideal and highly compressed gas. The water, air, and detonation gas are simulated using the Eulerian technique in a FEM program. Since the bubble dynamics is affected strongly by the hydrostatic pressure of the surrounding water, the size of the water region is designed the same as that in the experiment. To make the simulation more realistic, an air domain is created in the model to prevent the water rise in the case of bubble expansion. The Eulerian boundary is fixed and applied non-reflecting type, this helps prevent the materials from flowing out of the model and the inaccuracy caused by the pressure wave reflection. To reduce the computational time as well as enhance the calculation accuracy, only the Eulerian domain surrounding the initial bubble has a fine mesh. Particularly, this domain is set

of 1.2 times the maximal bubble radius to leverage the simulation performance. The initial bubble position has the smallest mesh size which is chosen as 0.1 times the initial bubble radius. From the outside surface of the initial bubble to the boundary of the bubble region, the element size is gradually increased to the value of 0.1 times of maximal bubble radius. Of the research made, the other regions have an element size of 100 mm. The model with mesh strategy is described in **Fig. 4**. The eight nodes element, type EC3D8R, is used which allows simulating multi-materials in an element.

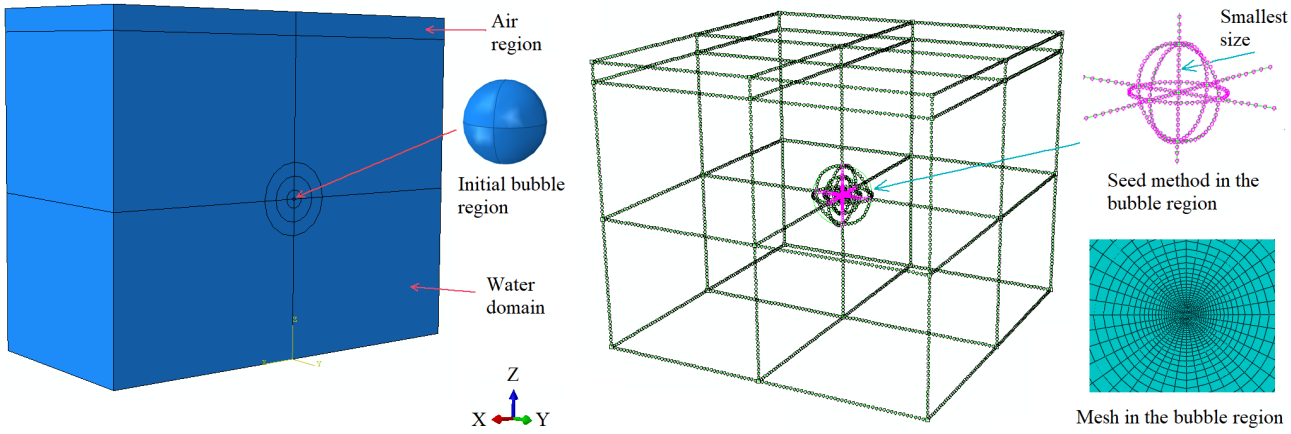

Fig. 4. The model of the bubble in the free water domain

Because the model contains an air region on the top of the water domain, the air pressure equals the initial hydrostatics pressure at the contact surface. The hydrostatic pressure is defined proportionally to the depth of the water domain. The input parameters of the initial bubble are determined based on Cole's calculation [1]. Since the explosive is assumed to be spherical, the initial bubble radius can be determined:

$$R = \left(\frac{3}{4\pi} \frac{W_c}{\rho_{ch}} \right)^{\frac{1}{3}}, \tag{7}$$

where W_c is the charge mass (kg), and ρ_{ch} is the density of the explosive.

Based on the calculation for detonation products of TNT presented in **Fig. 5**, the pressures are much higher at smaller specific volumes. When the specific volume is sufficiently large, the explosion gas can be assumed as an isentropic process with a specific heat ratio of 1.25. Because the bubble expands rapidly at the initial stage and the initial bubble radius is much smaller than the maximal radius, without losing the generalization about the bubble dynamics, the bubble is assumed to initiate at twice the charge radius in this study, corresponding to the eight times larger in the volume. Therefore, the density of the gas at the initial state can be calculated:

$$\rho_g = \frac{\rho_{ch}}{8} = \frac{1630}{8} = 203.75 \text{ kg/m}^3.$$

The specific volume of gas is inversely proportional to the density as:

$$v_g = \frac{1}{\rho_{ch}} = \frac{1}{203.75} = 0.00491 \text{ m}^3/\text{kg} = 4.91 \text{ cm}^3/\text{g}.$$

The exponential relation of a log-log plot (**Fig. 5**) can be expressed by the relation:

$$P_g = A v_g^{-\gamma}, \tag{8}$$

where P is pressure, v_g is specific volume, A and γ are constant.

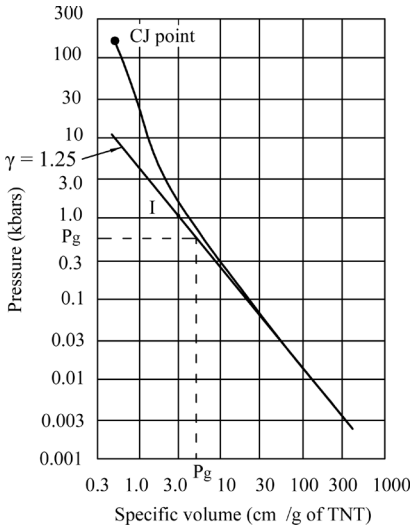

Fig. 5. The calculation for detonation products of TNT [1]

Because the specific volume of gas initiates at 4.91 cm^3/g, this value is sufficiently large to consider the gas is ideal, therefore the corresponding pressure of this specific density is:

$$P_g = 4.1456 v_g^{-1.25} = 4.1456(4.91)^{-1.25} = 0.5672 \text{ kbars} = 56720000 \text{ Pa}.$$

The hydrostatic pressure distribution in the water domain is defined by setting the values at the lowest and highest points, then the pressure at any point will be interpolated automatically by the software. Since the original coordinate system is set at the lowest point of the water domain, therefore, the pressure at the highest point is equal to atmospheric pressure in the air region, and the pressure at the lowest point (0, 0, 0) is determined as:

$$P_g = P_{atm} + \rho_w \cdot g \cdot h, \tag{9}$$

where P_{atm} is the atmospheric pressure, ρ_w is the water density, g is the gravitational acceleration, and h is the water depth.

Because the effect of heat exchange is negligible in studying the bubble dynamics [30], the physical process of the detonation gas product is considered to be adiabatic. Thus, the air and detonation gas in the numerical model can be simulated using the Mie-Grüneisen EOS which applies the Hugoniot's theory for reference curve [29]. This is also applicable for simulating the water, which is supposed to be incompressible, inviscid, and irrotational. **Table 1** provides the detail of the physical parameters of the model.

Table 1
The details of physical parameters

Parameters	Value	Unit
Water density (ρ_w)	1000	[Kg/m^3]
Sound speed in the water (c_w)	1500	[m/s]
Air density (ρ_a)	1.17	[Kg/m^3]
Ratio of specific heat of the air (γ_a)	1.4	–
Initial pressure of the air domain (P_{air})	1.0E5	[Pa]
Density of the explosive (TNT) (ρ_c)	1630	[Kg/m^3]
Density of the initial gas of the bubble (ρ_g)	203.75	[Kg/m^3]
Ratio of specific heat of the bubble (γ_g)	1.25	–
Initial pressure of the bubble (P_g)	5.672E7	[Pa]

3. Results and discussion

3. 1. Bubble in free field

In this section, the numerical results of the bubble dynamics in the free domain are analyzed and compared to the experimental results, BEM results, and analytical data for verification. Although the boundary condition of the numerical model is simplified and the shockwave propagation phase is not counted on the simulation, the FEM results provide valuable information on the behavior of the UNDEX bubble. **Fig. 6** illustrates similar bubble shapes among FEM bubble, BEM bubble, and experimental bubble at different time intervals in the case of 55 g TNT [31]. Since the lack of data for comparison, only bubble oscillation in the first cycle is considered in this paper. **Fig. 7–9** shows the bubble radius as a function of time in the first cycle for three charge masses (10, 35, and 55 g of TNT). In all cases, the bubble expands quickly at the early stage because the gas is compressed at high pressure. Subsequently, the internal pressure decreases rapidly because of the increase in the bubble volume. After reaching its maximal radius, the bubble begins to contract. At the final bubble contraction stage, the bubble radius decreases rapidly because of the increase in the surrounding flow inertia. The results on bubble radius and duration of the first bubble cycle are compared in **Table 2**. It can be seen that the experimental results are much larger than the FEM results. To be more detailed, the maximal radius error is 13.72 % in the case of 10 g TNT and the maximal error of bubble duration is 4.75 % in the case of 55 g TNT. However, the FEM results are compared well with the BEM results and the data using Rayleigh-Plesset theory with the estimation is less than 4 % for both maximal radius and duration of the first bubble circle [31]. This can be explained because the initial conditions of the bubble in FEM are determined based on Cole's calculation, in which the detonation gas product is assumed as an ideal gas. Therefore, this approximation may reduce the initial pressure of the inside gas. Besides, the experiments were conducted using Hexocire, whereas the BEM and FEM models were executed with the equivalent mass using TNT.

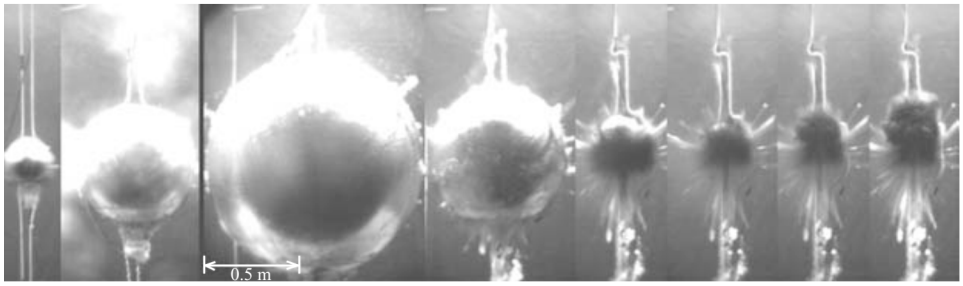

a

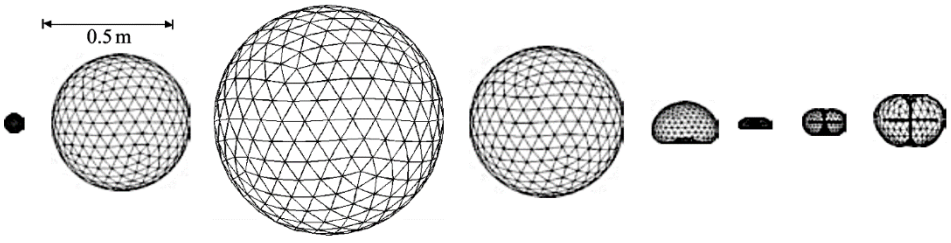

b

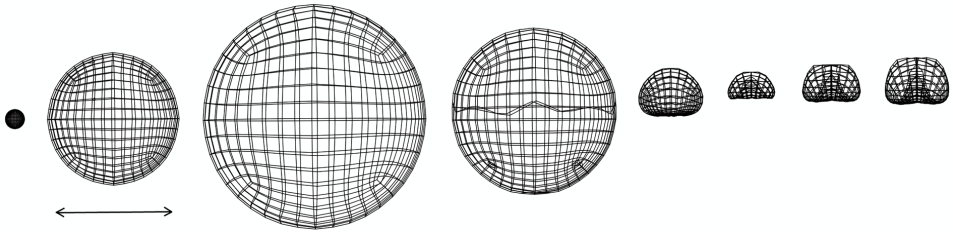

c

Fig. 6. Specific bubble shape at different time intervals:
a – Experimental results; *b* – BEM results; *c* – FEM results [27]

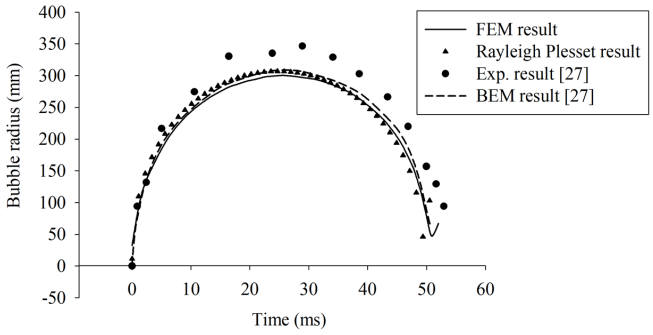

Fig. 7. The change of bubble radius when using 10 g TNT [27]

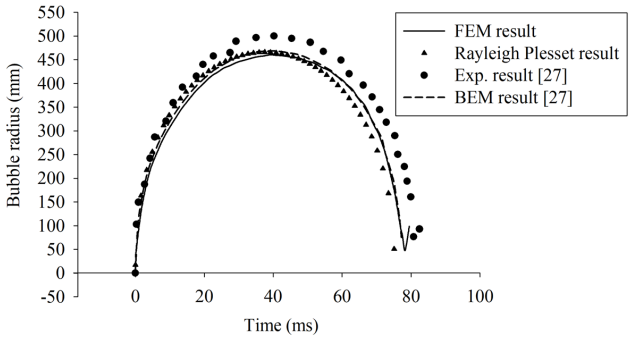

Fig. 8. The change of bubble radius when using 35 g TNT [27]

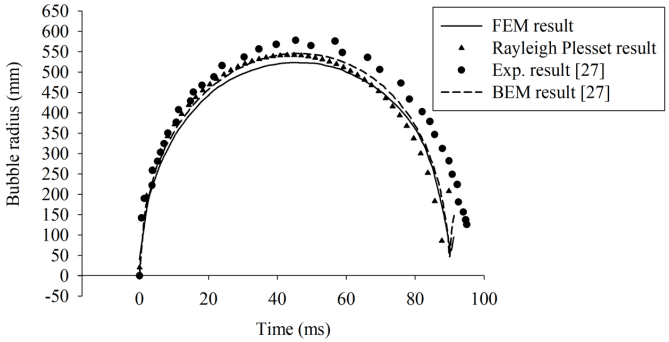

Fig. 9. The change of bubble radius when using 55 g TNT [27]

Table 2

The comparison of maximal bubble radius (R_m) and the duration of the first bubble cycle (T_c) between FEM and other methods

Method	R_m (m)	T_c (ms)	R_m error (%)	T_c error (%)
		W_c = 10 g		
Reyleigh Pleasset	0.3069	49.4	2.23	3.52
Exp.	0.3414	52.9	13.72	3.32
BEM	0.3087	50.6	2.83	1.17
FEM	0.3002	51.0	–	–
		W_c = 35 g		
Rayleigh Plesset	0.4659	75.1	1.17	3.84
Exp.	0.5001	80.7	8.60	3.33
BEM	0.4685	77.3	1.74	1.02
FEM	0.4605	78.1	–	–
		W_c = 55 g		
Reyleigh Pleasset	0.5416	87.7	3.51	3.20
Exp.	0.5778	94.9	9.57	4.75
BEM	0.5452	89.9	4.14	0.77
FEM	0.5226	90.6	–	–

3. 2. Bubble in the vicinity of a deformable wall

In order to investigate the behavior of the bubble as well as the deformable walls, the bubble model of 55 g TNT is developed to investigate the phenomenon of a bubble oscillating in the vicinity of a vertical or horizontal deformable wall. The arrangement of the numerical models is illustrated in **Fig. 10**, in which the model involves the Eulerian region containing water, air, and compressed gas, and the Lagrangian domain of a deformable wall. The bubble is positioned at the middle of the water domain with a distance (H) of 0.6 m from the wall. Since the present study only focuses on the case of a bubble near an infinite boundary, therefore the wall is chosen square with a side length of 1.5 m, which is pretty larger than the maximal bubble size. The thickness of the wall, T, will be varied to examine the effect of boundary stiffness on bubble development. The wall is meshed using 900 linear quadrilateral elements, S4R, and is fixed at four edges. The Eulerian region has a meshing strategy as described in the sub-section below, which includes 1,173,872 elements, type EC3D8R. For solving the interaction between the Eulerian and Lagrangian regions, the General contact in Abaqus software is applied to allow automatic implementation. The wall is made of steel and the mechanical properties are shown in **Table 3**.

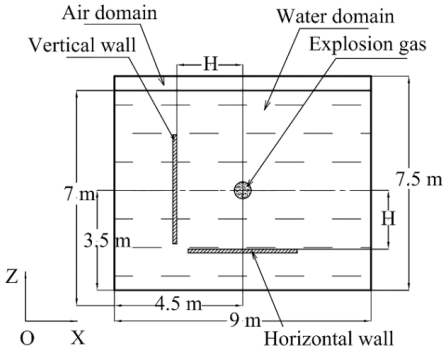

Fig. 10. The arrangement of the numerical model of a bubble nearby a vertical or horizontal deformable wall

Table 3
Physical parameters of the wall

Parameter	Value	Unit
Density (ρ_s)	7800	Kg/m^3
Young's modulus (E)	210	GPa
Poisson's ratio (v)	0.3	–
Yielding stress (σ_s)	240	MPa

3. 2. 1. Bubble dynamics near a vertical wall

In the case of a bubble oscillating near a wall, the bubble behavior is affected by the buoyancy forces in an upward direction and the Bjerknes forces, which act towards the wall. The specific bubble shapes at different times during the first cycle are shown in **Fig. 11**. It can be seen that the proposed model can simulate necessary features of a bubble nearby a deformable structure, including the expansion, contraction, and collapse phase with the water jet development towards the wall. To investigate the behavior of the deformable wall during the bubble oscillation, the displacement of the wall center relative to its initial position is examined at different stiffness (**Fig. 12**). The negative value shows the displacement of the wall towards the bubble and the positive value shows the displacement in the inverse direction. In the case $T = 2$ mm, the wall behaves like a compliant wall. The displacement of the wall center mainly obeys the expansion and contraction of the bubble. When the bubble expands, the wall center moves away, and as the bubble contracts, the wall center moves toward the bubble. However, when $T = 15$ and 30 mm, the stiffness of the wall increases, the oscillation frequency of the wall center increases.

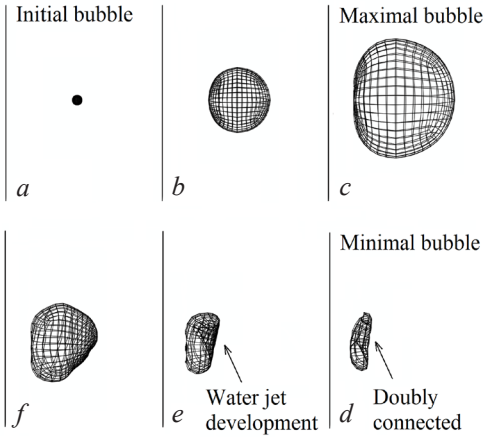

Fig. 11. The bubble shape in the case of nearby a vertical deformable wall ($T = 30$ mm) at different intervals: $a - t = 0$, $b - t = 8.1$; $c - t = 44.2$; $d - t = 96.5$ ms; $e - t = 97.2$; and $f - t = 97.8$ ms

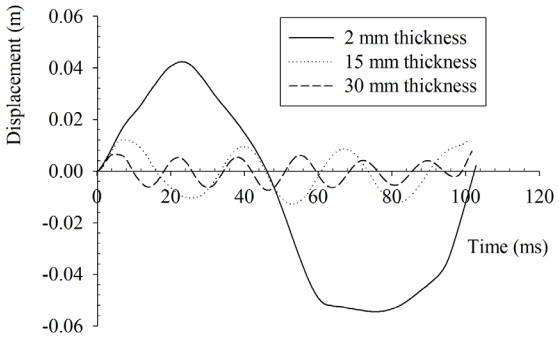

Fig. 12. The displacement of the wall center relative to its initial position of a bubble near a vertical deformable wall

To examine the influence of the stiffness of the wall on the water jet development, the water jet development is analyzed at the doubly connected bubbles. During the bubble contraction, different bubble parts move at various rates because of the imbalance in the ambient pressure. Since the wall is on the left of the bubble and the hydrostatic pressure is higher at lower points, the lower left part of the bubble contracts faster, this results in the left-bottom surface deforming into a bias water jet. The angles between the water jet and the horizontal direction at the double bubble connection are shown in **Fig. 13**, which occur at 92.7, 94.1, 96.5, and 97.2 ms concerning the wall thickness of 2, 15, 30 mm, and the rigid wall.

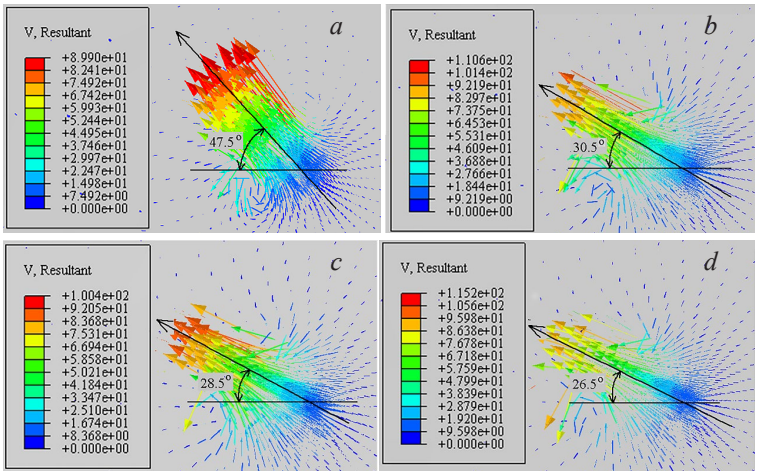

Fig. 13. The water jet direction in the case of the bubble near a vertical deformable wall (the wall on the left of the bubble): $a - T = 2$ mm; $b - T = 15$ mm; $c - T = 30$ mm; d – rigid wall

It can be seen that the maximum angle is 47.50 in the case of $T = 2$ mm and the minimum angle is 26.50 as the bubble near a rigid wall. These point out that when the wall stiffness increases, the Bjerknes force increase, leading to the decrease in the water jet angle. Besides, it is realized that the minimum of the bubble occurs earliest with the 2 mm thickness wall. This indicates that the increase in the wall stiffness may lengthen the first bubble cycle.

3. 2. 2. Bubble dynamics above a horizontal wall

In the case of a bubble fluctuating above a deformable wall, the Bjerknes forces are downward to the wall while the buoyancy forces are in the inverse direction. Therefore, the bubble behavior and the water jet development are affected by the dominant forces. Although the difference in the relative position between the wall and the bubble, the wall behaves in a similar trend to the case of the bubble near a vertical wall. The wall deforms like a compliant one when the thickness is 2 mm and the oscillation frequency of the wall center increases as the stiffness increases (**Fig. 14**). The displacement of the wall center is nearly the same as that of the bubble near a vertically deformable wall. This means the deformation of the wall is caused by the motion of the bubble ambient flow rather than the attractive forces from the bubble.

The bubble shape at different time intervals in its first cycle is shown in **Fig. 15**.

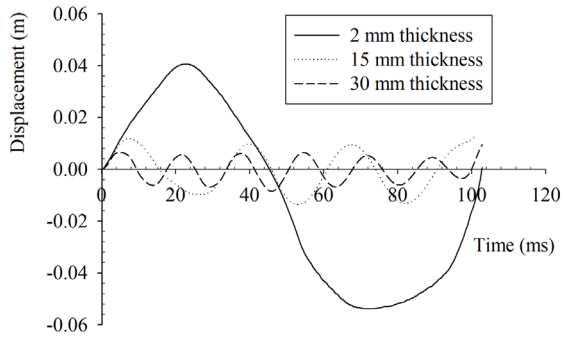

Fig. 14. The displacement of the wall center relative to its initial position of a bubble above a deformable wall

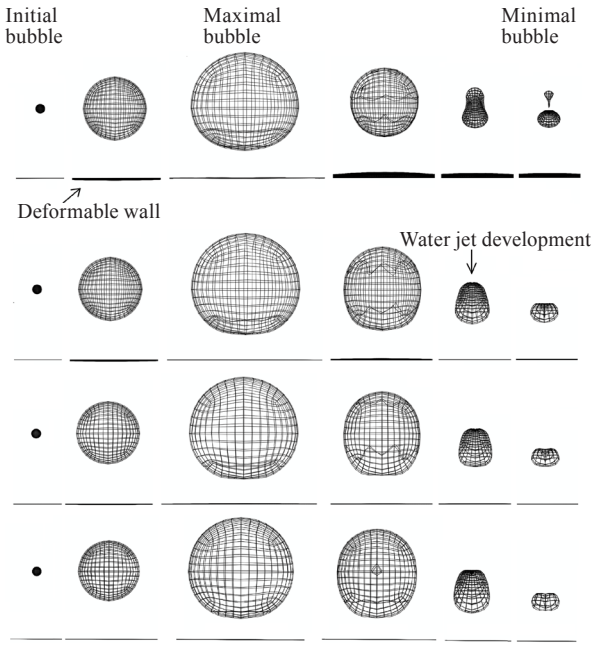

Fig. 15. The development of a bubble above a deformable wall during the first circle. From top-down, $T = 2$, 15, 30 mm and rigid wall; the minimal bubble occurs at 91.6, 94.8, 97.1, and 97.8 ms respectively

The bubbles experience similar expansion and contraction periods in all case studies. However, in case $T = 2$ mm, the bubble is necked and split into two-part during the bubble collapse phase because the buoyancy and Bjerknes forces are equivalent. In the case $T = 15, 30$ mm, and the rigid wall, the upper parts of the bubble deform faster because the Bjerknes forces are dominated, therefore the water jet develops downward. However, the Bjerknes is not strong enough, therefore no doubly connected bubble is formed during the first cycle. Besides, there is no consistent data of bubble centroid displacement is investigated among the simulations. The minimum volume of the bubble occurs at 91.6, 94.8, 97.1, and 97.8 ms relative to the case of $T = 15, 30$ mm, and the rigid wall. This once again confirms that the increase in the wall stiffness may cause a longer duration of the bubble circle.

3. 3. Bubble below a complex surface

For further studying the large-scale model, a numerical bubble model of 100 kg of TNT below a simplified ship is developed. The numerical model is arranged as **Fig. 16**, in which a simplified ship model is designed based on the middle part of an actual ship, including 10 stiffeners (springs) and a keel with the cross-section of a T-beam (**Fig. 17**). The bubble is initiated directly below the middle of the ship. **Table 4** details the dimensions of the stiffeners and the keel and the thickness of the shell is chosen as 25 mm. The mechanical properties of the plate and beam are described in **Table 3**. The air domain inside the hull girder is created by dividing the Eulerian domain into partitions in which the hull girder surface plays as the interface surface. Then the partition inside will be assigned material of the air and the outside one will be assigned water. The «General contact» is applied to all interface surfaces for coupling different regions. The model includes 1080448 elements, type EC3D8R for the Eulerian domain, and 5526 elements, type S4R. Since the present research focuses on studying the phenomenon of a bubble below a complex surface, therefore the effect of shockwave on the structure in the early stage of the bubble process is not counted on the simulation and the ship model is fixed at two ends during the simulation.

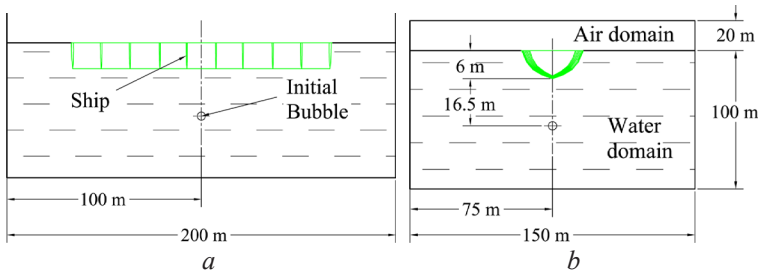

Fig. 16. The arrangement of the numerical model of a bubble below a ship: *a* – side view (longitudinal view); *b* – cross-section view (Transverse view)

Table 4
Beam dimensions (m)

Parameter	b	h	t_f	t_w
Stiffener	0.12	0.15	0.012	0.012
Keel	0.18	0.2	0.014	0.014

The interaction between the UNDEX bubble and structures is of considerable interest because it involves several events, and the bubble influences the structure over a long period. **Fig. 18** illustrates the state of the simplified ship and the bubble at various time intervals, in which the color contour illustrates the ship's deformation. The bubble initiates spherically as in **Fig. 18, *a***. During the first period, the rapid expansion of the bubble causes the surrounding flow to move and pushes the ship upwards (**Fig. 18, *b***). The bubble becomes the largest reaches at around 293.5 ms with a radius of 5.16 m (**Fig. 18, *c***). Then the bubble starts to contract because of the imbalance between the pressure of the inside gas and the pressure of the surrounding

flow (**Fig. 18, *d***), this pulls the ship downwards to the bubble. At the time of 661.5 ms, the bubble becomes toroidal and reaches its minimal volume (**Fig. 18, *e***), after that the bubble rebounds again for another oscillation process (**Fig. 18, *f***). It also can be realized that the bubble duration in the first circle is longer than that of the bubble in the free domain, which is 592 ms when using the Rayleigh-Plesset equation [31]. This can be explained that the influence of the ship may slow down the bubble contraction rate.

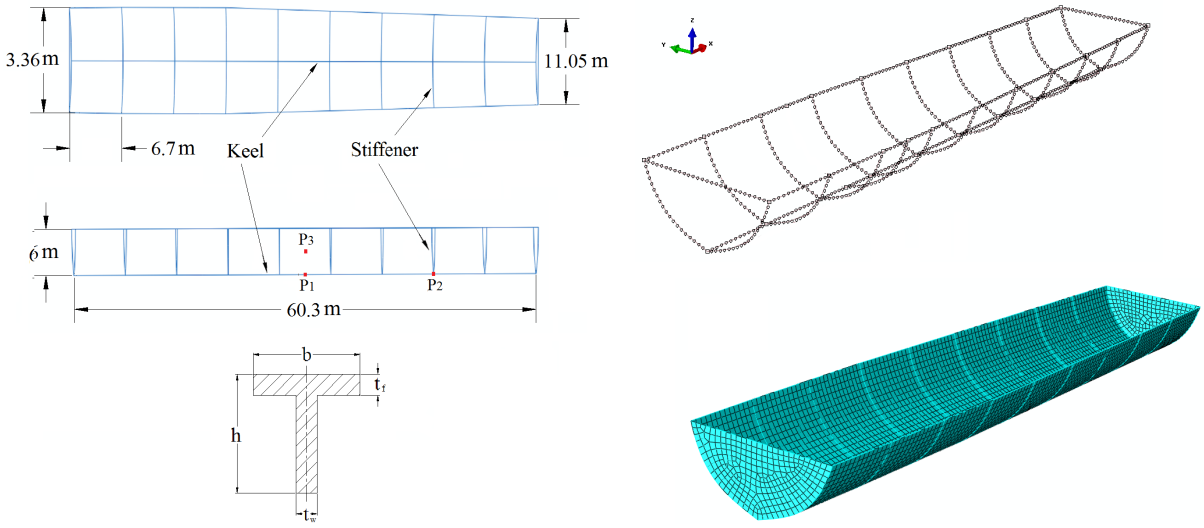

a *b*

Fig. 17. Specifications of simplified ship model: *a* – top view and side view; *b* – 3D numerical model

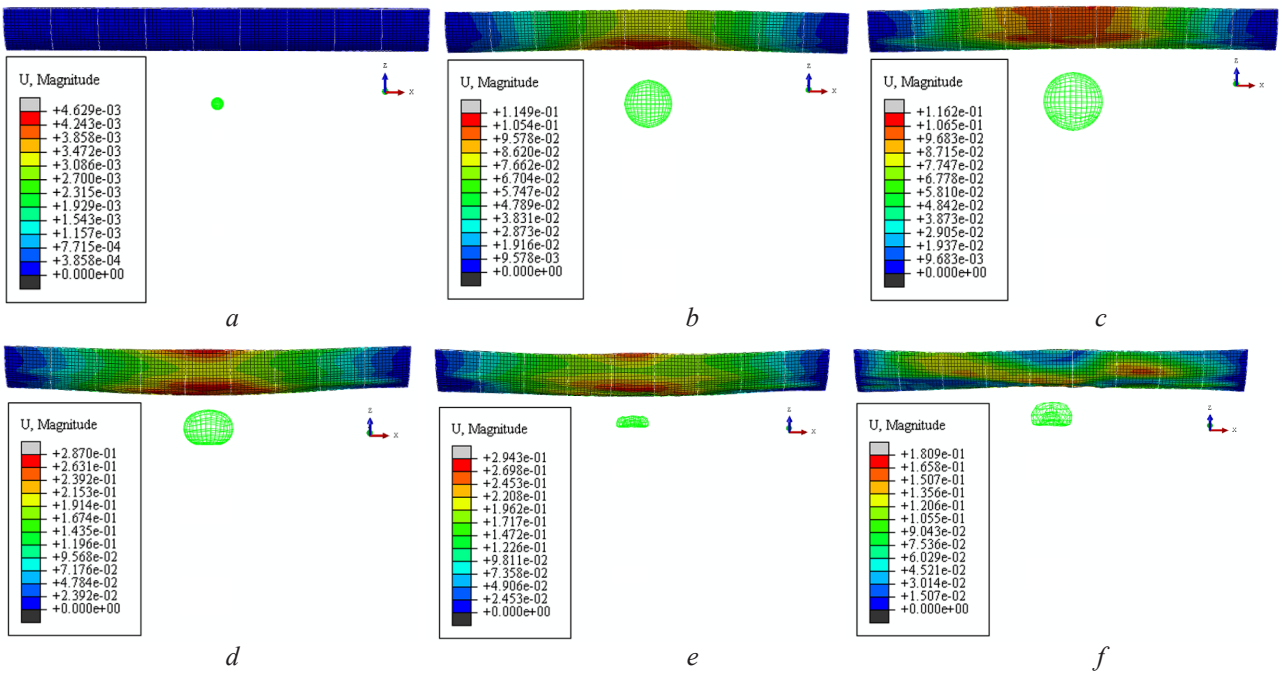

a *b* *c*

d *e* *f*

Fig. 18. The bubble shape and the ship's deformation at different time intervals: *a* – $t = 4.5$; *b* – $t = 108$, *c* – $t = 293.5$; *d* – $t = 549$; *e* – $t = 661.5$; *f* – $t = 801$ ms with the scale factor of 5

The deflection of the ship keel at different time intervals is shown in **Fig. 19, *a***, and **Fig. 19, *b*** describes the displacement of a typical point (P1) on the ship. The positive value shows

the motion far away and the negative value shows the motion toward the bubble. Numerical results show that the keel takes on its vertical fluctuation, which is also known as the whipping effect. This phenomenon may cause serious damage to the ship and exceed that caused by the primary shockwave.

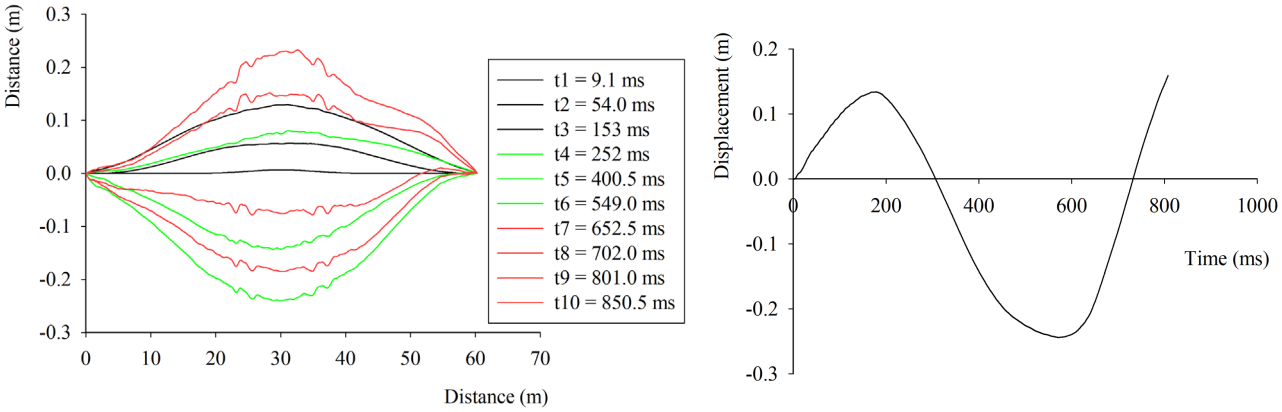

a *b*

Fig. 19. The deformation of the ship keel: *a* – the whipping deflection of the ship keel at different time intervals; *b* – the displacement of a typical point (P1) on the structure during the first bubble circle

The application of CEL in ABAQUS also provides valuable information about the contact pressure transmitting from the Eulerian elements to the Lagrangian structure, this allows investigating the mechanical damage of nearby structures.

Fig. 20 shows the contact pressure at three points on the ship: P1 is the point at the middle of the simplified ship, P2 is the point above P1 and at the side of the ship, and P3 is a point at the horizontal direction from P1 (**Fig. 17**). It can be seen that the smallest pressure occurs at the farthest point, P3. This can be explained because of the loss in energy during the transmission of the pressure waves in the water, therefore the pressure magnitude decreases corresponding to the increase in the traveling distance. The magnitude of pressure at P1 is slightly higher than that at P2 during the early period (about 600 ms), however, they reflect a similar trend. This is because P1 and P2 are in the same motion direction of the bubble. The numerical results also show a peak pressure at P1 during the bubble collapse phase, the magnitude is about 2.3E7 Pa at around 700 ms. This peak may be caused by the water-jet attack because P1 is in the water-jet direction. This once again confirms that the nearby structure may be suffered serious damage because of the resonance of several factors.

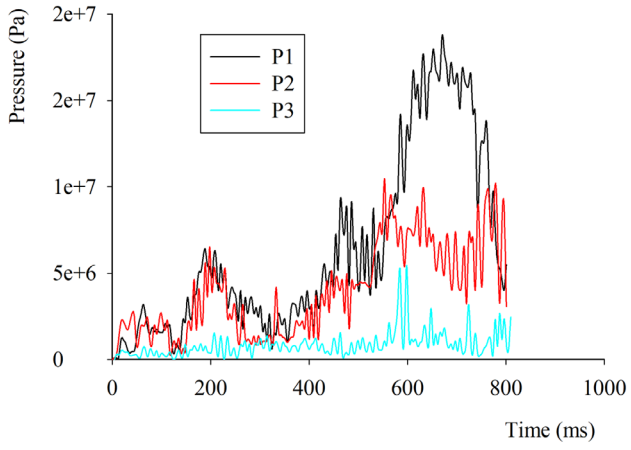

Fig. 20. The contact pressure at different points on the structure

3. 4. Limitations and research development directions

Although the proposed method has successfully simulated major features of the bubble oscillation nearby the structures, however, in order to reproduce the model for further study or application in practice, the researchers should carefully consider the following problems:

– to reduce the computational time while still obtaining the calculation accuracy, the Eulerian domain around the initial bubble should be meshed smaller than the other regions;

– because the effect of shockwave on the structure at the early stage of the bubble process is not counted in this simulation, therefore the total deformation of the structure might be larger in the real experiment;

– since the detonation gas product is considered as an ideal and highly compressed gas, the water is supposed to be incompressible, inviscid, and irrotational, and the effect of heat exchange is negligible in this study, this may affect the accuracy of the bubble duration as well as the bubble size.

Therefore, future studies should focus on the effect of the meshing technique, heat exchange, and the properties of fluid and gas. Such studies would require deep theories but would also investigate valuable information about the UNDEX phenomenon.

4. Conclusions

This paper presents a numerical method of FEM to investigate the interaction of the bubble and the deformable structure, in which the CEL technique in commercial software is developed to solve the FSI problem. The numerical model of a UNDEX bubble is first developed and verified by comparing results with experimental, BEM, and empirical data. The maximal radius error is 13.72 % and the maximal error of bubble duration is 4.75 % in comparison with experimental results and less than 4 % in comparison with the BEM results for both the maximal radius and duration of the first bubble circle. Then, the bubble models are extended to study the bubble dynamics in different scenarios. When the bubble is nearby a vertical or a horizontal deformable wall, the Bjerknes effect becomes stronger when the stiffness of the structure increases. This influences the water jet development during the collapse phase. The maximum water jet angle is 47.50 and the minimum angle is 26.50 in the case of a bubble near a 2 mm-vertical deformable wall and rigid wall respectively. The results also point out that the increase in the structure's stiffness may lengthen the duration of the first bubble cycle, the minimum of the bubble occurs the latest with the rigid wall. In further investigation, the proposed method is developed to study the bubble oscillating below a complex structure. The bubble becomes the largest at around 293.5 ms with a radius of 5.16 m and reaches its minimal volume at the time of 661.5 ms. The numerical model successfully reproduced crucial effects of the bubble on the structure, including the whipping effect, water jet attacks, and pressure pulse during the bubble collapse. The peak pressure occurs at the point in the waterjet direction during the bubble collapse phase, the magnitude is about 2.3E7 Pa at around 700 ms. These show the important effects of UNDEX bubble pulsation on structural damage. Despite limitations related to simplifications of the numerical model, the proposed approach presents a reliable method for studying the UNDEX bubble phenomenon using a multi-material Eulerian hydrocode formulation along with the CEL technique. The proposed approach can be applied to different explosive charges, weights, depths, and materials. It also provides itself as a powerful tool for design, evaluation, and optimization.

Conflict of interest

The author declared no potential conflicts of interest concerning the research, authorship, and publication of this article.

Financing

The study was performed without financial support.

Data availability

Data will be made available on reasonable request.

References

[1] Cole, R. H. (1948). Underwater explosions. Princeton: Princeton University Press. doi: https://doi.org/10.5962/bhl.title.48411

[2] Zhang, Y. L., Yeo, K. S., Khoo, B. C., Chong, W. K. (1998). Three-Dimensional Computation of Bubbles Near a Free Surface. Journal of Computational Physics, 146 (1), 105–123. doi: https://doi.org/10.1006/jcph.1998.6042

[3] Pearson, A., Cox, E., Blake, J. R., Otto, S. R. (2004). Bubble interactions near a free surface. Engineering Analysis with Boundary Elements, 28 (4), 295–313. doi: https://doi.org/10.1016/s0955-7997(03)00079-1

[4] Lundgren, T. S., Mansour, N. N. (1991). Vortex ring bubbles. Journal of Fluid Mechanics, 224, 177–196. doi: https://doi.org/10.1017/s0022112091001702

[5] Wang, Q. X., Yeo, K. S., Khoo, B. C., Lam, K. Y. (1996). Nonlinear interaction between gas bubble and free surface. Computers & Fluids, 25 (7), 607–628. doi: https://doi.org/10.1016/0045-7930(96)00007-2

[6] Wang, Q. X., Yeo, K. S., Khoo, B. C., Lam, K. Y. (2005). Vortex ring modelling of toroidal bubbles. Theoretical and Computational Fluid Dynamics, 19 (5), 303–317. doi: https://doi.org/10.1007/s00162-005-0164-6

[7] Zhang, Y. L., Yeo, K. S., Khoo, B. C., Wang, C. (2001). 3D Jet Impact and Toroidal Bubbles. Journal of Computational Physics, 166 (2), 336–360. doi: https://doi.org/10.1006/jcph.2000.6658

[8] Han, R., Zhang, A., Liu, Y. (2015). Numerical investigation on the dynamics of two bubbles. Ocean Engineering, 110, 325–338. doi: https://doi.org/10.1016/j.oceaneng.2015.10.032

[9] Wang, C., Khoo, B. C., Yeo, K. S. (2003). Elastic mesh technique for 3D BIM simulation with an application to underwater explosion bubble dynamics. Computers & Fluids, 32 (9), 1195–1212. doi: https://doi.org/10.1016/s0045-7930(02)00105-6

[10] Barras, G., Souli, M., Aquelet, N., Couty, N. (2012). Numerical simulation of underwater explosions using an ALE method. The pulsating bubble phenomena. Ocean Engineering, 41, 53–66. doi: https://doi.org/10.1016/j.oceaneng.2011.12.015

[11] Zhang, A., Wang, S., Huang, C., Wang, B. (2013). Influences of initial and boundary conditions on underwater explosion bubble dynamics. European Journal of Mechanics - B/Fluids, 42, 69–91. doi: https://doi.org/10.1016/j.euromechflu.2013.06.008

[12] Duncan, J. H., Milligan, C. D., Zhang, S. (1996). On the interaction between a bubble and a submerged compliant structure. Journal of Sound and Vibration, 197 (1), 17–44. doi: https://doi.org/10.1006/jsvi.1996.0515

[13] Zhang, A. M., Yao, X. L., Li, J. (2008). The interaction of an underwater explosion bubble and an elastic–plastic structure. Applied Ocean Research, 30 (3), 159–171. doi: https://doi.org/10.1016/j.apor.2008.11.003

[14] Zong, Z., Wang, J., Zhou, L., Zhang, G. (2015). Fully nonlinear 3D interaction of bubble dynamics and a submerged or floating structure. Applied Ocean Research, 53, 236–249. doi: https://doi.org/10.1016/j.apor.2015.09.011

[15] Zhang, A. M., Wu, W. B., Liu, Y. L., Wang, Q. X. (2017). Nonlinear interaction between underwater explosion bubble and structure based on fully coupled model. Physics of Fluids, 29 (8), 082111. doi: https://doi.org/10.1063/1.4999478

[16] Zhang, A. M., Yao, X. L., Feng, L. H. (2009). The dynamic behavior of a gas bubble near a wall. Ocean Engineering, 36 (3-4), 295–305. doi: https://doi.org/10.1016/j.oceaneng.2008.12.006

[17] He, Z., Chen, Z., Jiang, Y., Cao, X., Zhao, T., Li, Y. (2020). Effects of the standoff distance on hull structure damage subjected to near-field underwater explosion. Marine Structures, 74, 102839. doi: https://doi.org/10.1016/j.marstruc.2020.102839

[18] Gan, N., Liu, L. T., Yao, X. L., Wang, J. X., Wu, W. B. (2021). Experimental and numerical investigation on the dynamic response of a simplified open floating slender structure subjected to underwater explosion bubble. Ocean Engineering, 219, 108308. doi: https://doi.org/10.1016/j.oceaneng.2020.108308

[19] Wu, W., Liu, M., Zhang, A.-M., Liu, Y.-L. (2021). Fully coupled model for simulating highly nonlinear dynamic behaviors of a bubble near an elastic-plastic thin-walled plate. Physical Review Fluids, 6 (1). doi: https://doi.org/10.1103/physrevfluids.6.013605

[20] Klaseboer, E., Khoo, B. C., Hung, K. C. (2005). Dynamics of an oscillating bubble near a floating structure. Journal of Fluids and Structures, 21 (4), 395–412. doi: https://doi.org/10.1016/j.jfluidstructs.2005.08.006

[21] Mirjalili, S., Karimi, A., Hadi, S. (2006). Analysis of Underwater Explosion Bubble on Ship Structure. Modares Mechanical Engineering, 6 (1), 41–52. Available at: https://mme.modares.ac.ir/article-15-12037-en.html

[22] Zhang, Z., Wang, L., Yao, X., Lang, J. (2017). Dynamics of an Underwater Explosion Bubble near a Rigid Wall: Effect of Slenderness Ratio, Installation, and Distance Parameter. Journal of Coastal Research, 33 (4), 959–971. doi: https://doi.org/10.2112/jcoastres-d-16-00094.1

[23] Jin, Z., Yin, C., Chen, Y., Hua, H. (2019). Dynamics of an underwater explosion bubble near a sandwich structure. Journal of Fluids and Structures, 86, 247–265. doi: https://doi.org/10.1016/j.jfluidstructs.2019.02.022

[24] Wang, H., Cheng, Y. S., Liu, J., Gan, L. (2016). The Fluid-Solid Interaction Dynamics between Underwater Explosion Bubble and Corrugated Sandwich Plate. Shock and Vibration, 2016, 1–21. doi: https://doi.org/10.1155/2016/6057437

[25] Jin, Z., Yin, C., Chen, Y., Hua, H. (2018). Numerical study on the interaction between underwater explosion bubble and a moveable plate with basic characteristics of a sandwich structure. Ocean Engineering, 164, 508–520. doi: https://doi.org/10.1016/j.oceaneng.2018.07.001

[26] Tian, Z., Liu, Y., Wang, S., Man Zhang, A., Kang, Y. (2019). Dynamic Response of Floating Body Subjected to Underwater Explosion Bubble and Generated Waves with 2D Numerical Model. Computer Modeling in Engineering & Sciences, 118 (2), 397–423. doi: https://doi.org/10.31614/cmes.2019.04419

[27] Zhang, Z., Wang, C., Zhang, A.-M., Silberschmidt, V. V., Wang, L. (2019). SPH-BEM simulation of underwater explosion and bubble dynamics near rigid wall. Science China Technological Sciences, 62 (7), 1082–1093. doi: https://doi.org/10.1007/s11431-018-9420-2

[28] Mair, H. U. (1999). Review: Hydrocodes for Structural Response to Underwater Explosions. Shock and Vibration, 6 (2), 81–96. doi: https://doi.org/10.1155/1999/587105

[29] Simulia ABAQUS 6.11, ABAQUS Analysis User's Manual (2011). Providence.

[30] Brown, K., Burns, S., Christon, M. (2002). Coupled Eulerian-Lagrangian Methods for Earth Penetrating Weapon Applications. United States. doi: https://doi.org/10.2172/808588

[31] Klaseboer, E., Hung, K. C., Wang, C., Wang, C. W., Khoo, B. C., Boyce, P. et al. (2005). Experimental and numerical investigation of the dynamics of an underwater explosion bubble near a resilient/rigid structure. Journal of Fluid Mechanics, 537 (1), 387. doi: https://doi.org/10.1017/s0022112005005306

Received date 20.10.2022
Accepted date 28.12.2022
Published date 19.01.2023

How to cite: *Nguyen, A.-T. (2023). A numerical research on the interaction between underwater explosion bubble and deformable structure using CEL technique. EUREKA: Physics and Engineering, 1, 134–151. doi: http://doi.org/10.21303/2461-4262.2023.002637*